Near unity ideality factor and Shockley-Read-Hall lifetime in GaN-on-GaN *p-n* diodes with avalanche breakdown

Zongyang Hu,[1,2,a)] Kazuki Nomoto,[1,2] Bo Song,[1,2] Mingda Zhu,[1,2] Meng Qi,[2] Ming Pan,[3] Xiang Gao,[3] Vladimir Protasenko,[1,2] Debdeep Jena,[1,2,4] and Huili Grace Xing[1,2,4,a)]
[1]*School of Electrical and Computer Engineering, Cornell University, Ithaca, New York 14853, USA*
[2]*Department of Electrical Engineering, University of Notre Dame, Notre Dame, Indiana 46556, USA*
[3]*IQE RF LLC, Somerset, New Jersey 08873, USA*
[4]*Department of Materials Science and Engineering, Cornell University, Ithaca, New York 14853, USA*

(Received 11 October 2015; accepted 17 November 2015; published online 15 December 2015)

Textbook-like device characteristics are demonstrated in vertical GaN *p-n* diodes grown on bulk GaN substrates. These devices show simultaneously an avalanche breakdown voltage (*BV*) of >1.4 kV under reverse bias, an ideality factor plateau of ~2.0 in a forward bias window followed by a near unity ideality factor of 1.1, which are consistently achieved over a temperature range of 300–400 K. At room temperature (RT), the diode with a mesa diameter of 107 μm showed a differential on-resistance R_{on} of 0.12 mΩcm^2, thus resulting in a record figure-of-merit BV^2/R_{on} of ~16.5 GW/cm^2, which is the highest ever demonstrated in any semiconductors. Analytical models are used to fit experimental *I-Vs*; based on the recombination current with an ideality factor of ~2.0, a Shockley-Read-Hall lifetime of 12 ns is extracted at RT with an estimated recombination center concentration of 3×10^{15} cm^{-3}. © *2015 AIP Publishing LLC*.
[http://dx.doi.org/10.1063/1.4937436]

As Si-based electronics approach their performance limit due to material properties, wide band gap semiconductors such as SiC and GaN have become attractive for next generation power devices. GaN combines a heterostructure capability with a large band gap, a high critical electric field with high electron mobility, a large saturation velocity, and an excellent thermal conductivity and is therefore considered as an ideal solution for efficient power conversion applications. Lateral GaN power devices on foreign substrates such as sapphire, SiC, and Si have already shown promising high frequency and high power performance.[1–3] However, the true advantage of wide band gap devices in high power conversion is realized with the use of bulk single crystal GaN substrates. This allows vertical epitaxy and active regions of devices to be developed with very few dislocations and defects. The characteristics of a *p-n* junction diode are among the most sensitive probes of material properties and device design. GaN based *p-n* junction diodes on GaN substrates with high breakdown voltage (*BV*) and low on-resistance (R_{on}) have been shown, and their performance is approaching the material-limited figure-of-merit (FOM) for GaN unipolar devices.[4–7] However, the ideality factor of GaN *p-n* junction diodes is usually large due to excessive leakage through defects and/or high series resistances; values between 1 and 2 are rarely reported.[6–10]

In this letter, vertical GaN *p-n* homojunction diodes on bulk GaN substrates with an ideality factor near unity (~1.1) are demonstrated, which enables reliable extraction of Shockley-Read-Hall (SRH) lifetime in high quality GaN. Temperature-dependent *I-V* measurements show consistent near-unity ideality factors and avalanche breakdown behavior.

The diodes studied in this work were grown epitaxially by metalorganic chemical vapor deposition (MOCVD) on a bulk GaN substrate with a dislocation density of ~10^6 cm^{-2}. The epitaxial structure has a p^{++} GaN cap for anode ohmic contacts, a 400 nm GaN:Mg (Mg: 1×10^{19} cm^{-3}) layer, an 8 μm GaN:Si (Si: 1–2 $\times$ 10^{16} cm^{-3}) drift region, and a 0.2 μm GaN:Si (Si: 1×10^{18} cm^{-3}) buffer layer. The completed device structure is shown schematically in Fig. 1. Edge termination is realized by a beveled mesa, spin-on-glass (SOG) passivation, and field plate. The detailed device fabrication process is reported elsewhere.[7,10] The *p*-GaN layer has a hole concentration of 7×10^{16} cm^{-3} and a hole mobility of 24 cm^2/V·s as determined by Hall effect measurements. It is found that the forward *I-V* characteristics are the same for diodes with and without field plates (Fig. 1), while the reserve bias breakdown is significantly improved in diodes with field plates.[7,10] To minimize the effects of parasitic capacitance, the capacitance-voltage (*C-V*) measurements were carried out on devices without field plates. The diode size is defined by the bottom diameter of the mesa unless otherwise noted.

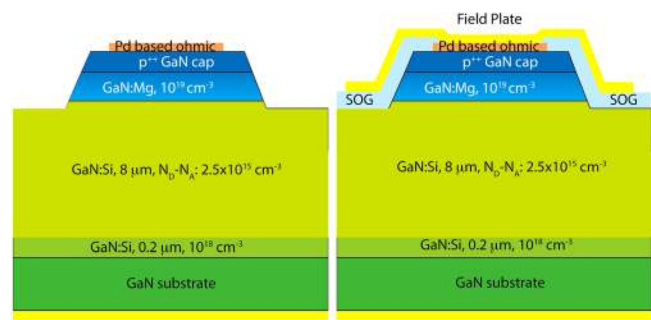

FIG. 1. Schematic cross-sections of GaN p–n junction diodes: (left) without passivation/field plates and (right) with field plates.

a)Electronic addresses: zh249@cornell.edu and grace.xing@cornell.edu

 © 2015 AIP Publishing LLC

This article is copyrighted as indicated in the article. Reuse of AIP content is subject to the terms at: http://scitation.aip.org/termsconditions. Downloaded to IP: 128.84.244.134 On: Tue, 15 Dec 2015 16:29:26

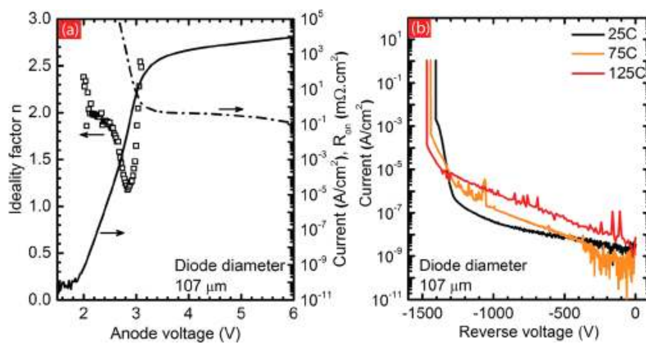

FIG. 2. (a) Forward *I-V* characteristics at RT measured on GaN *p-n* diodes with a mesa diameter of 107 μm and an effective diameter of 117 μm (due to current spreading). (b) Temperature dependent reverse *I-V* characteristics and breakdown voltages.

Figure 2(a) shows the representative forward *I-V* characteristics of GaN *p-n* junction diodes with a diameter of 107 μm at the bottom of the mesa, measured at room temperature (RT). Assuming an effective diameter of 117 μm taking into account current spreading outside the mesa,[10] a forward current close to 9.3 kA/cm^2 is measured at 6 V, while a differential $R_{on} \sim 0.12$ mΩcm^2 is calculated. The on/off current ratio is about 14 orders of magnitude (limited by our measurement setup), thanks to minimized defects in GaN. The extracted ideality factor shows a very clear transition from $\sim$2.0 at 2 V to $\sim$1.1 at 2.8 V. Figure 2(b) shows the temperature-dependent reverse-bias *I-V* measured on diodes with field plates. *BV* increases with increasing temperature: 1406 V at RT, 1442 V at 350 K, and 1470 V at 400 K. The positive coefficient of *BV* versus temperature is a signature of avalanche breakdown, which is desired for reliable device operation for high power applications. The higher leakage current at higher temperatures suggests that trap-assisted conduction is most likely the dominating leakage mechanism. The Baliga-FOM is calculated to be $\sim$16.5 GW/cm^2 at RT, a record high of all the GaN power p-n diodes ever reported.

Using a *C–V* analysis (Fig. 3(a)), the built-in voltage of the *p-n* junction is extracted to be $\sim$3.0 V, which is consistent with the net doping concentrations in the diodes in this study. With N_D and N_A denoting the donor and acceptor concentrations, respectively, the net carrier concentration N_D-N_A of the *n*-GaN drift region is determined to be $\sim 1.8 \times 10^{15}$ cm^{-3} close to the metallurgical junction, and $\sim 2.5 \times 10^{15}$ cm^{-3} deeper in the drift region. Given the target Si concentration of 1–2 $\times 10^{16}$ cm^{-3}, the compensating acceptor level is estimated to be $\sim 10^{16}$ cm^{-3}, which is among the lowest achieved in MOCVD GaN.[6,7]

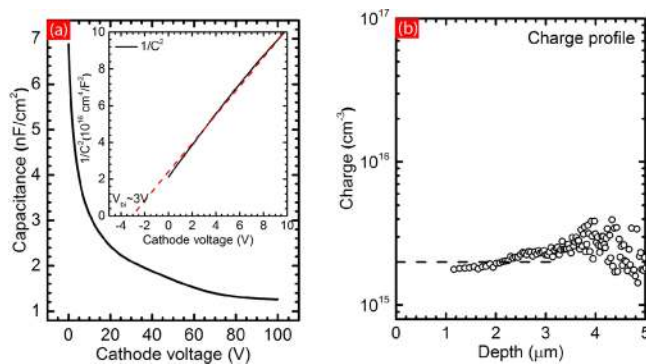

FIG. 3. (a) *C-V* characteristics of GaN *p-n* junction diodes without passivation at 100 kHz at RT, inset: $1/C^2$ vs. *V* plot of the *p-n* junction, (b) net carrier concentration extracted from the *C-V* measurement.

The *I-V* characteristics of a *p-n* junction diode can be expressed as

$$J = J_{d0}(e^{qV_a/kT} - 1) + J_{nr0}(e^{qV_a/2kT} - 1) + J_{r0}(e^{qV_a/kT} - 1). \quad (1)$$

The 1st term represents the diffusion current density (J_d) with an ideality factor η of $\sim$1, the 2nd term is the SRH recombination current density (J_{nr}) inside the depletion region with an η of $\sim$2, and the 3rd term is the *radiative* recombination current density (J_r) inside the depletion region with an η of $\sim$1. J_{d0}, J_{nr0}, and J_{r0} represent the bias insensitive term of diffusion and recombination currents, V_a is the voltage applied over the intrinsic junction: $V_a = V - JR_{sp}$, and R_{sp} is the total specific parasitic resistance of the diode.

Figure 4(a) shows experimentally measured *I-V* curves with three calculated components for comparison. The band-to-band *radiative* recombination current inside the depletion region is expressed as: $J_{r0} = 2qbn_i^2W$, where n_i is the intrinsic carrier concentration in GaN, b is the radiative recombination coefficient, and W is the width of the depletion region. Based on the reported radiative recombination coefficients in GaN,[11] J_r is negligible compared with the other two current components in the entire voltage range. It is worth noting that the excitonic radiative recombination current in the depletion region is not accounted for, which will be scrutinized in future studies. Based on the arguments above, the non-radiative SRH recombination is thus concluded to be the dominant recombination mechanism. The SRH recombination rate can be written as[12]

$$U_{SRH} = \frac{pn - n_i^2}{(n + n_1)\tau_{p0} + (p + p_1)\tau_{n0}}, \quad (2)$$

where τ_{n0} (τ_{p0}) is the electron (hole) lifetime, n_1 (p_1) is the calculated electron (hole) concentration if the Fermi level is at the trap energy level E_t. Under forward bias $n_i \ll (n+p)$, the contribution from n_1 and p_1 is small unless the trap state

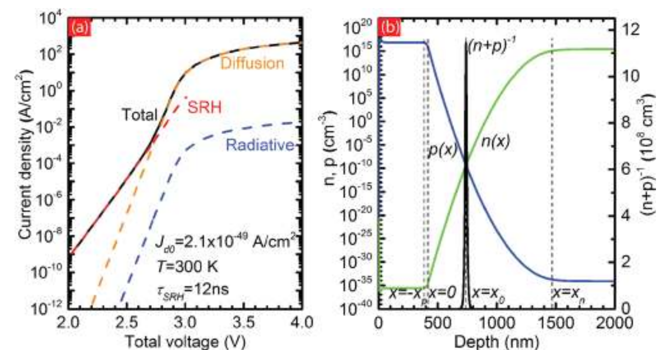

FIG. 4. (a) Diffusion, band-to-band radiative recombination, and SRH recombination current components of a GaN *p-n* junction using the fitting parameters extracted from experimental *I-V* characteristics in this work. (b) 1-D simulation of carrier concentration distribution inside a GaN *p-n* junction at 0 V, with the peak in black highlighting the plane where $n = p$.

This article is copyrighted as indicated in the article. Reuse of AIP content is subject to the terms at: http://scitation.aip.org/termsconditions. Downloaded to IP: 128.84.244.134 On: Tue, 15 Dec 2015 16:29:26

energies are sufficiently close to the band edge. The fact that $\eta \sim 2$ is experimentally measured for the recombination dominated region of the forward *I-Vs* suggests that it is most probably valid to assume a near mid-gap trap state dominates the SRH recombination current. Provided that recombination does not cause significant deviation of carrier concentrations inside the depletion region, i.e., $np = n_i^2\exp(qV_a/kT)$ holds, it is clear from Eq. (2) that the highest recombination rate occurs at the plane where $n\tau_{p0} = p\tau_{n0}$.

Figure 4(b) shows the simulated carrier profiles inside the depletion region at 0 V. The peak in $(n+p)^{-1}$ located at x_0 shows the plane with the highest recombination rate ($\tau_{p0} = \tau_{n0}$ is assumed). The distribution of carriers near the plane is

$$n(x) = \sqrt{\frac{\tau_{n0}}{\tau_{p0}}} n_i e^{qV_a/2kT} e^{qE_0(x-x_0)/kT}, \quad p(x) = \sqrt{\frac{\tau_{p0}}{\tau_{n0}}} n_i e^{qV_a/2kT} e^{-qE_0(x-x_0)/kT}, \tag{3}$$

where $x = 0$ denotes the metallurgic p-n junction plane, E_0 is the magnitude of electric field near $x = x_0$. The recombination current can thus be written as

$$\begin{aligned} J_{nr} &= 2q\int_{-x_p}^{x_n} \frac{n_i^2\left(e^{qV_a/kT}-1\right)}{\tau_{p0}n(x)+\tau_{n0}p(x)}dx \\ &\approx q\int_{-\infty}^{\infty} \frac{1}{\tau_{SRH}} \frac{n_i\left(e^{qV_a/2kT}-e^{-qV_a/2kT}\right)}{\cosh\left[qE_0(x-x_0)/kT\right]}dx \\ &= \frac{2\pi kTn_i}{\tau_{SRH}E_0}\sinh\left(\frac{qV_a}{2kT}\right), \end{aligned} \tag{4}$$

where $\tau_{SRH} = \sqrt{\tau_{n0}\tau_{p0}}$ is used. The factor of 2 comes from contributions from both electron and hole currents.[12] The integral limits are extended approximately to infinity based on the fact that the denominator increases sharply when the integral is moved away from $x = x_0$. Under low injection approximation, on the *n*-side of the depletion region, there is

$$n(x) = N_d e^{-\frac{1}{2}q^2N_d(x_n-x)^2/(\varepsilon kT)}, \quad p(x) = \frac{n_i^2}{N_d} e^{qV_a/kT} e^{\frac{1}{2}q^2N_d(x_n-x)^2/(\varepsilon kT)}, \tag{5}$$

where N_d is the net doping concentration in the *n*-region, and ε is the dielectric constant of GaN. By setting $\tau_{p0}n(x) = \tau_{n0}p(x)$, the electric field can be solved as

$$\begin{aligned} E_0 &= \left[\frac{N_dkT\left(\ln\tau_{p0} - \ln\tau_{n0} + 2\ln N_d - 2\ln n_i - qV_a/kT\right)}{\varepsilon}\right]^{1/2} \\ &\approx \left[\frac{N_dkT(2\ln N_d - 2\ln n_i - qV_a/kT)}{\varepsilon}\right]^{1/2}. \end{aligned} \tag{6}$$

It can be seen that E_0 decreases with increasing temperature and forward bias. In order to determine carrier transport properties from the measured diode *I-Vs*, the temperature-dependent bandgap values of GaN are adopted from the previous reports:[11,13] 3.42 eV at 300 K, 3.40 eV at 350 K, and 3.37 eV at 400 K. Figure 5(b) shows the forward *I-V* characteristics of the GaN *p-n* diodes with a mesa diameter of 707 μm. The diode shows a R_{on} of $\sim$2 mΩ·cm^2 largely invariant within the temperature window of 300 K–400 K, which is much higher than R_{on} of the 107 μm diode. The strong dependence of R_{on} on the diode area[7,10] is possibly due to various edge effects such as current crowding and photon recycling.[14] Therefore, modeling of the diode *I-V* in the entire voltage window of 1–4 V in this work is limited to the large area diodes, for which these edge effects are minimized.

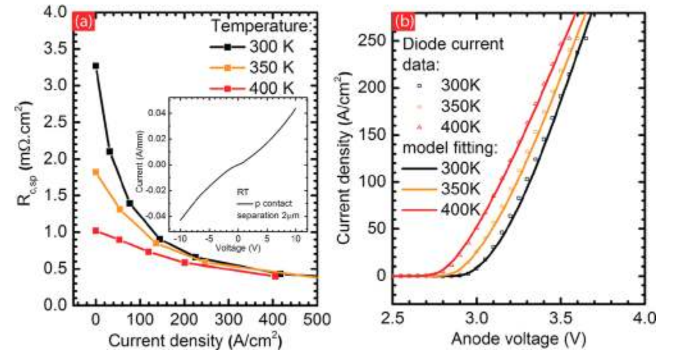

FIG. 5. (a) Temperature-dependent specific contact resistance on *p*-GaN extracted from the TLM measurements. Inset: *I-V* characteristic measured on two *p*-GaN contacts separated by 2 μm. (b) Forward *I-V* characteristics of GaN *p-n* diodes at 300 K, 350 K, and 400 K in linear scale: symbols are experimentally measured data, and solid lines are modeled results.

To improve accuracy of the modeling, the contact resistance of *p*-GaN is measured as a function of temperature and current density. The specific contact resistance ($R_{c,sp}$) and current density are measured by the transfer length method (TLM) and calculated by using the effective contact area (the contact width W times the transfer length L_T). In Fig. 5(a), due to a slight non-linearity in the *I-V* curve of the *p*-GaN contacts, the extracted $R_{c,sp}$ shows a strong dependence on current density at RT: 3.3 mΩcm^2 at low current density and $\sim$0.4 mΩcm^2 at 500 A/cm^2. $R_{c,sp}$ reduces at higher temperatures, likely due to thermal activation of Mg acceptors in *p*-GaN. The *I-Vs* of the *p-n* diodes are thus fitted (Fig. 5(b)) by considering $R_{c,sp}$ and series resistances from both *p* and *n* regions (the *n*-GaN substrate resistance is included in the total resistance of n-GaN: r_n), which are summarized in Table I. High injection effects including conductivity modulation and photon recycling are considered *insignificant* in Fig. 5(b), since the diode size is large and the current density level is reasonably low (<300 A/cm^2). It is worth noting that the contact resistances do not play a role in modeling the diode *I-V* in the subthreshold region (up to the unity ideality factor, Fig. 6).

TABLE I. Fitting parameters in modeling of the GaN *p-n* diodes.

T (K)	r_p (mΩ cm^2)	r_n (mΩ cm^2)	μ_n (cm^2/V s)	J_{d0} (A/cm^2)	J_{nr0} (A/cm^2)	τ_{SRH} (ns)
300	0.13	1.7	1470	2.1×10^{-49}	2.7×10^{-26}	12
350	0.06	1.8	1380	3.9×10^{-41}	5.3×10^{-22}	15
400	0.04	1.9	1310	8.0×10^{-35}	8.9×10^{-19}	18

This article is copyrighted as indicated in the article. Reuse of AIP content is subject to the terms at: http://scitation.aip.org/termsconditions. Downloaded to IP: 128.84.244.134 On: Tue, 15 Dec 2015 16:29:26

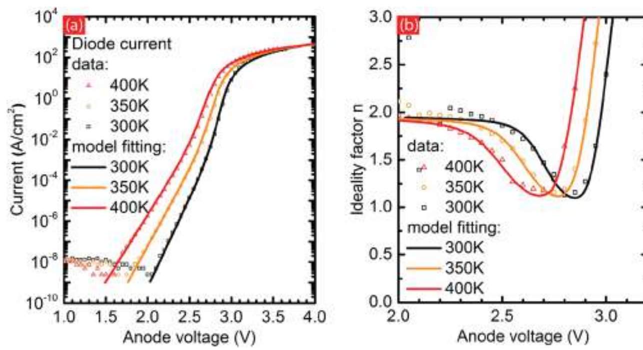

FIG. 6. (a) Forward *I-V* characteristics and (b) ideality factors of GaN *p-n* diodes from experiments (symbols) and modeling (lines).

The measured semi-log scale *I-V*s are plotted together with the modeled *I-V*s in Fig. 6(a). The leakage current floor of $\sim10^{-8}$ A/cm^2 is limited by the measurement system, while the intrinsic leakage current of the device is $<10^{-10}$ A/cm^2 as shown in Fig. 2. The low current levels ($J < 10^{-3}$ A/cm^2) can be modeled well for each temperature with a single τ_{SRH}, which is $\sim$12 ns at RT and increases slightly with increasing temperature. The dependence of the SRH lifetime on temperature is in agreement with an empirical power-law relation with a temperature coefficient $\alpha = 1.4$;[15] however, the underlying mechanism deserves a separate study. These numbers are also much higher than the reported lifetimes of electron and hole in Ref. 16, further confirming that the quality of epitaxial *n*-GaN grown on bulk GaN substrates is dramatically enhanced over time. Since SRH recombination is most sensitive to mid-gap centers, and the plane of the maximum recombination rate is located inside *n*-GaN in a $p+/n-$ junction, the SRH lifetime can be used to estimate the deep-level defect concentration in *n*-GaN. Using $\tau_{SRH} = 1/(n_t v_{th} \sigma)$, the extracted SRH lifetime of 12 ns, a thermal velocity v_{th} of 2.6×10^7 cm/s at 300 K, and a capture cross-section $\sigma \sim 10^{-15}$ cm^2,[17] a mid-gap recombination center concentration n_t of 3×10^{15} cm^{-3} is found. This trap concentration is in the same order of magnitude with the compensating center concentration estimated based on the Si doping and extracted net carrier concentration N_D-N_A.

In Fig. 6(b), the ideality factors extracted from the forward *I-V*s are plotted. The minimal ideality factors at various temperatures are $\sim$1.1, and the corresponding voltages are shifted due to the increase in the intrinsic carrier concentration n_i at elevated temperatures. Also tabulated in Table I are the extracted electron mobility, diffusion, and SRH current coefficients. An electron mobility of $\sim$1500 cm^2/V s in n-GaN, with a net carrier concentration of $\sim2 \times 10^{15}$ cm^{-3} and a compensation concentration of $\sim1 \times 10^{16}$ cm^{-3}, is comparable to the recent report.[6] It is also seen that the modeled ideality factor plateaus at values slightly lower than 2 due to the decrease of E_0 with a higher junction voltage, which causes J_{nr0} to increase. SRH lifetime is typically field dependent,[18] however, the calculated values of E_0 in this device are <0.02 MV/cm for a forward bias >2 V. Hence, the low E_0 values allow for the accurate modeling with a single SRH lifetime for each temperature. At RT, the extracted diffusion current coefficient is $J_{d0} \sim 2 \times 10^{-49}$ A/cm^2, lower than the value reported for 6H-SiC *p-n* junctions[19] because of the larger band gap of GaN. Near unity ideality factors in GaN observed over a temperature window have never been reported previously. The near unity ideality factor is enabled by two primary facts: (1) a small SRH recombination current inside the depletion region due to a long SRH recombination lifetime, i.e., low concentrations of recombination centers; (2) low parasitic resistances allow diffusion current ($\eta = 1$) to dominate over a wide bias window.

GaN *p-n* junction diodes with R_{on} of $\sim$0.12 mΩcm^2 and $BV > 1.4$ kV with avalanche capability are demonstrated. Ideality factors as low as 1.1 are extracted at various temperatures, and values between 2 and 1 are measured for a forward voltage range of 2–3 V. A combination of low R_{on} and near-unity ideality factors signifies the *n*-GaN quality is high with low defect concentrations, a high electron mobility, and minority lifetime. It is shown that GaN *p-n* diodes can have near-ideal *I-V* characteristics described completely by analytical models. This is enabled by optimized MOCVD growths on low-dislocation-density single-crystal bulk GaN substrates. Carefully tuned device processes with properly designed edge termination and low contact resistances are also important in achieving low ideality factors. The long SRH lifetime and low R_{on} in GaN demonstrated in this work indicate possibilities to design GaN *p-n* diodes utilizing the bipolar benefits of the material. Performance far beyond the unipolar limit predicted by FOM might be achievable in GaN bipolar power devices.

This work was partly supported by the ARPAe SWITCHES project monitored by Tim Heidel.

[1]H. Xing, Y. Dora, A. Chini, S. Heikman, S. Keller, and U. K. Mishra, IEEE Electron Device Lett. **25**, 161 (2014).
[2]A. Margonenos, A. Kurdoghlian, M. Micovic, K. Shinohara, D. F. Brown, A. L. Corrion, H. P. Moyer, S. Burnham, D. C. Regan, R. M. Grabar, C. McGuire, M. D. Wetzel, R. Bowen, P. S. Chen, H. Y. Tai, A. Schmitz, H. Fung, A. Fung, and D. H. Chow, in *Compound Semiconductor Integrated Circuit Symposium* (2014), p. 1.
[3]M. Zhu, B. Song, M. Qi, Z. Hu, K. Nomoto, X. Yan, Y. Cao, W. Johnson, E. Kohn, D. Jena, and H. G. Xing, IEEE Electron Device Lett. **36**, 375 (2015).
[4]K. Nomoto, T. Nakamura, N. Kaneda, T. Kawano, T. Tsuchiya, and T. Mishima, in *Proceedings of ISCSRM* (2011), p. 1299.
[5]I. C. Kizilyalli, A. P. Edwards, H. Nie, D. Disney, and D. Bour, IEEE Trans. Electron Devices **60**, 3067 (2013).
[6]I. C. Kizilyalli, A. P. Edwards, O. Aktas, T. Prunty, and D. Bour, IEEE Trans. Electron Devices **62**, 414 (2015).
[7]K. Nomoto, Z. Hu, B. Song, M. Zhu, M. Qi, R. Yan, V. Protasenko, E. Imhoff, J. Kuo, N. Kaneda, T. Mishima, T. Nakamura, D. Jena, and H. G. Xing, IEEE IEDM **2015**, 9.7.
[8]J. M. Shah, Y. L. Li, T. Gessmann, and E. F. Schubert, J. Appl. Phys. **94**, 2627 (2003).
[9]C. A. Hurni, O. Bierwagen, J. R. Lang, B. M. McSkimming, C. S. Gallinat, E. C. Young, D. A. Browne, U. K. Mishra, and J. S. Speck, Appl. Phys. Lett. **97**, 222113 (2010).
[10]K. Nomoto, B. Song, Z. Hu, M. Zhu, M. Qi, N. Kaneda, T. Mishima, T. Nakamura, D. Jena, and H. G. Xing, "1.7 kV and 0.55 m$\Omega \cdot$cm^2 GaN p-n diodes on bulk GaN substrates with avalanche capability" IEEE Electron Device Lett. (unpublished).
[11]A. Dmitriev and A. Oruzheinikov, J. Appl. Phys. **86**, 3241 (1999).
[12]C. T. Sah, R. N. Noyce, and W. Shockley, Proc. IRE **45**, 1228 (1957).

This article is copyrighted as indicated in the article. Reuse of AIP content is subject to the terms at: http://scitation.aip.org/termsconditions. Downloaded to IP: 128.84.244.134 On: Tue, 15 Dec 2015 16:29:26

[13]O. Ambacher, J. Smart, J. R. Shealy, N. G. Weimann, K. Chu, M. Murphy, W. J. Schaff, L. F. Eastman, R. Dimitrov, L. Wittmer, M. Stutzmann, W. Rieger, and J. Hilsenbeck, J. Appl. Phys. **85**, 3222 (1999).
[14]K. Mochizuki, K. Nomoto, Y. Hatakeyama, H. Katayose, T. Mishima, N. Kaneda, T. Tsuchiya, A. Terano, T. Ishigaki, T. Tsuchiya, R. Tsuchiya, and T. Nakamura, IEEE IEDM **2011**, 26.3.1.
[15]M. S. Tyagi and R. Van Overstraeten, Solid-State Electron. **26**, 577 (1983).
[16]K. Kumakura, T. Makimoto, N. Kobayashi, T. Hashizume, T. Fukui, and H. Hasegawa, Appl. Phys. Lett. **86**, 052105 (2005).
[17]P. Hacke, T. Detchprohm, K. Hiramatsu, N. Sawaki, K. Tadatomo, and K. Miyake, J. Appl. Phys. **76**, 304 (1994).
[18]A. Schenk, Solid-State Electron. **35**, 1585 (1992).
[19]T. Kimoto, N. Miyamoto, and H. Matsunami, IEEE Trans. Electron Devices **46**, 471 (1999).

This article is copyrighted as indicated in the article. Reuse of AIP content is subject to the terms at: http://scitation.aip.org/termsconditions. Downloaded to IP: 128.84.244.134 On: Tue, 15 Dec 2015 16:29:26